


SCIENTIFIC REPORTS

OPEN

Towards high throughput GPCR crystallography: *In Meso* soaking of Adenosine A_{2A} Receptor crystals

Prakash Rucktooa¹, Robert K. Y. Cheng^{1,2}, Elena Segala¹, Tian Geng¹, James C. Errey¹, Giles A. Brown¹, Robert M. Cooke¹, Fiona H. Marshall¹  & Andrew S. Doré¹

Here we report an efficient method to generate multiple co-structures of the A_{2A} G protein-coupled receptor (GPCR) with small-molecules from a single preparation of a thermostabilised receptor crystallised in Lipidic Cubic Phase (LCP). Receptor crystallisation is achieved following purification using a low affinity “carrier” ligand (theophylline) and crystals are then soaked in solutions containing the desired (higher affinity) compounds. Complete datasets to high resolution can then be collected from single crystals and seven structures are reported here of which three are novel. The method significantly improves structural throughput for ligand screening using stabilised GPCRs, thereby actively driving Structure-Based Drug Discovery (SBDD).

Many of the world’s top selling drugs target G protein-coupled receptors (GPCRs)¹ for indications including inflammatory, neurological, gastrointestinal, cardiovascular and respiratory diseases². Structural data on this clinically relevant membrane protein superfamily has increased dramatically over the last decade, resulting from pioneering research from a number of groups^{3,4}. High resolution crystal structures are now available for almost all major GPCR classes and are transformative from a pharmaceutical perspective, with several drug candidates generated by structure-based drug design (SBDD) techniques^{5,6}. Nevertheless, GPCR crystallography throughput lags behind that of soluble targets (e.g. kinases)⁷, in part due to the inherent conformational flexibility and instability of GPCRs when removed from the native cell membrane environment. To overcome this, receptors have been thermostabilised by introducing a small number of targeted point mutations using the StaR[®]⁸, SABRE⁹ or CHESS¹⁰ technologies, or other mutagenesis approaches^{11–13}. These mutations enhance apparent thermostability and stabilise receptors in a specific pre-defined conformation, and detergent-resistant form¹⁴. Such approaches were instrumental in solving structures of members of class B and C GPCRs^{2,15,16}. Receptors stabilised using the StaR[®] technology rely less on stability conferred by high affinity ligands to increase the chance of crystallogenesis. Co-crystal structures are thus obtainable even with low affinity compounds and fragments¹⁷ identified in early stages of discovery projects. This provides a unique opportunity to apply soaking techniques, successfully utilised for soluble targets (e.g. kinases), to GPCR crystals grown *in meso* by lipidic cubic phase crystallisation (LCP). The reliable production of multiple co-structures on a regular basis, in step with the medicinal chemistry cycle time, is fully enabling for SBDD.

Here, we report an *in meso* crystal soaking method developed to improve the crystallographic throughput for our work with the adenosine A_{2A} receptor (A_{2A}R), including drug discovery activities. Previously, each ligand complex structure required a separate, bespoke A_{2A}R-ligand protein preparation. Now a single protein preparation can yield high resolution structural data for A_{2A}R in complex with up to a dozen different ligands. This also significantly minimises ligand amounts required to generate co-structures compared to using bespoke A_{2A}R-ligand protein preparations.

Theophylline binds to the thermostabilised receptor used for crystallisation (A_{2A}-StaR2-*b*_{RIL562}), with relatively low affinity ($pK_D = 5.71$), and with fast kinetics¹⁸, whereas potent A_{2A}R-selective antagonists such as 1,2,4-triazine derivatives¹⁹, typically bind with higher affinity ($pK_D > 8$) and exhibit slow off-rates. Despite its low affinity for A_{2A}-StaR2-*b*_{RIL562}, theophylline provides some thermostabilisation to the receptor in comparison to *apo* protein (Fig. 1A). This *in meso* soaking method uses theophylline as a low affinity carrier ligand, present throughout purification, to provide crystallisation-grade A_{2A}-StaR2-*b*_{RIL562} (Fig. 1B). The A_{2A}-StaR2-*b*_{RIL562}-Theophylline complex

¹Heptares Therapeutics Ltd, BioPark, Broadwater Road, Welwyn Garden City, Hertfordshire, AL7 3AX, UK. ²Present address: LeadXpro, Park InnovAARE, 5232, Villigen, Switzerland. Prakash Rucktooa, Robert K. Y. Cheng and Elena Segala contributed equally to this work. Correspondence and requests for materials should be addressed to F.H.M. (email: fiona.marshall@heptares.com)

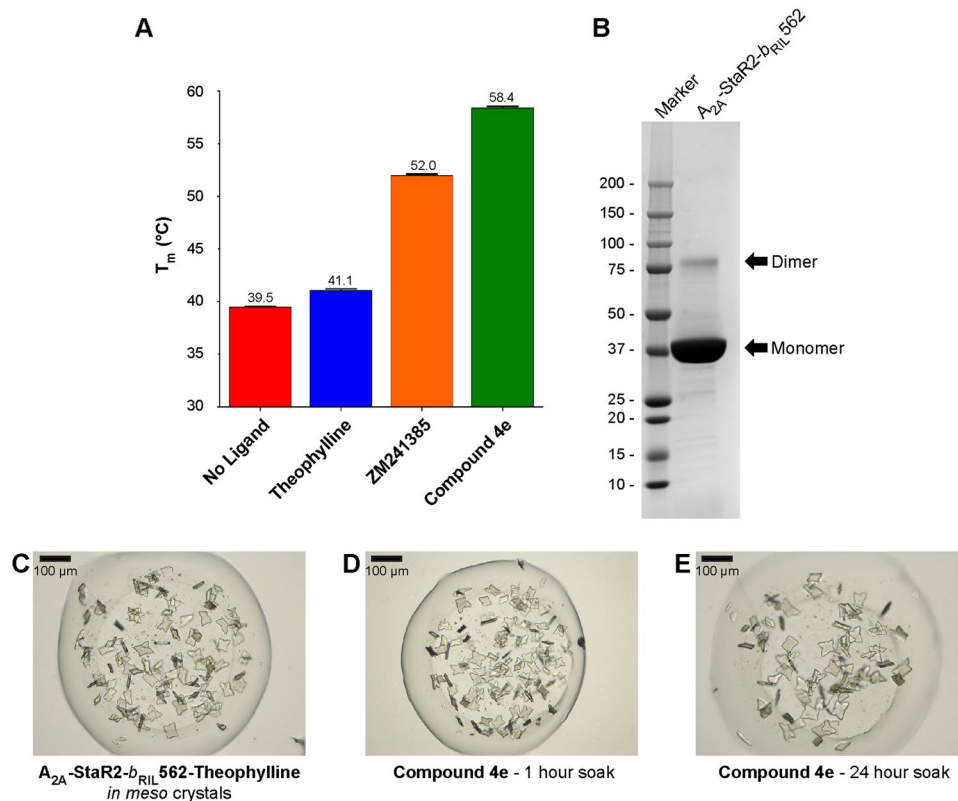


Figure 1. A_{2A}-StaR2-b_{RIL}562 Crystal Soaking. **(A)** Bar chart showing the melting temperature of A_{2A}-StaR2-b_{RIL}562 in its *apo* form or in the presence of theophylline, ZM241385 or Compound 4e, reflecting the relative stability of each protein preparation. **(B)** SDS-PAGE of concentrated A_{2A}-StaR2-b_{RIL}562 protein prior to crystallisation. **(C)** Crystals of the A_{2A}-StaR2-b_{RIL}562-Theophylline complex. **(D)** A_{2A}-StaR2-b_{RIL}562-Theophylline crystals following a 1 hour soak in 1 mM Compound 4e. **(E)** A_{2A}-StaR2-b_{RIL}562-Theophylline crystals following a 24 hour soak in 1 mM Compound 4e.

readily crystallises *in meso* yielding thick ~60 μm long plates (Fig. 1C), typically diffracting to 2.0 Å and containing a theophylline molecule in the A_{2A}R orthosteric binding site²⁰ (Fig. 2A). Crystals with theophylline have also been used previously to generate a structure with another xanthine, PSB36²⁰.

The utility of the *in meso* soaking system for diverse ligands from chemical series other than xanthines was then investigated. A_{2A}-StaR2-b_{RIL}562-Theophylline crystals were soaked in mother liquor supplemented with A_{2A} antagonists **Tozadenant**²¹ (pK_D = 8.4), **LUAA47070**²² (pK_D = 6.5) or **Vipadenant**²³ (pK_D = 9.0), and their diffraction characterised. Crystals from these experiments diffracted in spacegroup C222₁ to 2.0–3.1 Å resolution (Table 1). **Tozadenant**, **LUAA47070** and **Vipadenant** are all well defined in the electron density maps (Fig. 2B–D). For these ligands the basal region of the orthosteric site is delimited by Trp246^{6,48}, which engages in Van der Waals contacts to the **Tozadenant** benzothiazole ring, the **LUAA47070** thiazole ring or the **Vipadenant** furan ring (Fig. 2B–D). These ligands explore different regions at the apical end of the orthosteric site. The 4-hydroxy,4-methylpiperidine moiety of **Tozadenant** sits upright on the benzothiazole ring, and hydrogen bonds to Thr256^{6,58}. The N,2,2-trimethylpropanamide group of **LUAA47070** extends obliquely towards transmembrane helix 1 (TM1), and engages in water-mediated contacts with ECL2 Glu169 and Tyr9^{1,35}. Further this structure shows how the experimentally defined water mediated interactions of the amide group of **LUAA47070** to both Asn253^{6,55} and His278^{7,42} contribute to this ligand binding pose. Finally, the **Vipadenant** 2-methylaniline moiety points laterally towards TM1, and is hydrogen-bonded to Tyr9^{1,35}. We find that, despite adopting a range of orientations in the orthosteric binding site, ligands from different chemical series can be effectively soaked into A_{2A}-StaR2-b_{RIL}562-Theophylline crystals, and used in crystallographic structural studies to identify their binding modes. Contrary to poorly diffracting, bespoke A_{2A}-StaR2-b_{RIL}562-**Tozadenant** crystals, likely resulting from the disruption of the salt bridge between extracellular loop 2 (ECL2) Glu169 and ECL3 His264, interfering with crystal packing, co-crystals from soaking experiments yielded good quality structural data, highlighting the versatility of the *in meso* soaking system.

The validity of structural results obtained by the *in meso* soaking method was checked using **ZM241385**²⁴ (pK_D = 8.6), a well-characterised A_{2A}R antagonist that increases A_{2A}-StaR2-b_{RIL}562 stability by ~12 °C (Fig. 1A). The crystal structure of the receptor in complex with ZM241385 resulting from *in meso* soaking, was compared with similar complexes obtained from bespoke crystallisation setups using either A_{2A}-StaR2-b_{RIL}562²⁵ or A_{2A}-b_{RIL}562²⁶ (Fig. 2E). Overlaying these structures shows a remarkably similar structural conformation of residues in the orthosteric located within 5 Å of the ligand with an all atom r.m.s.d. of only 0.074 Å (soaked v/s

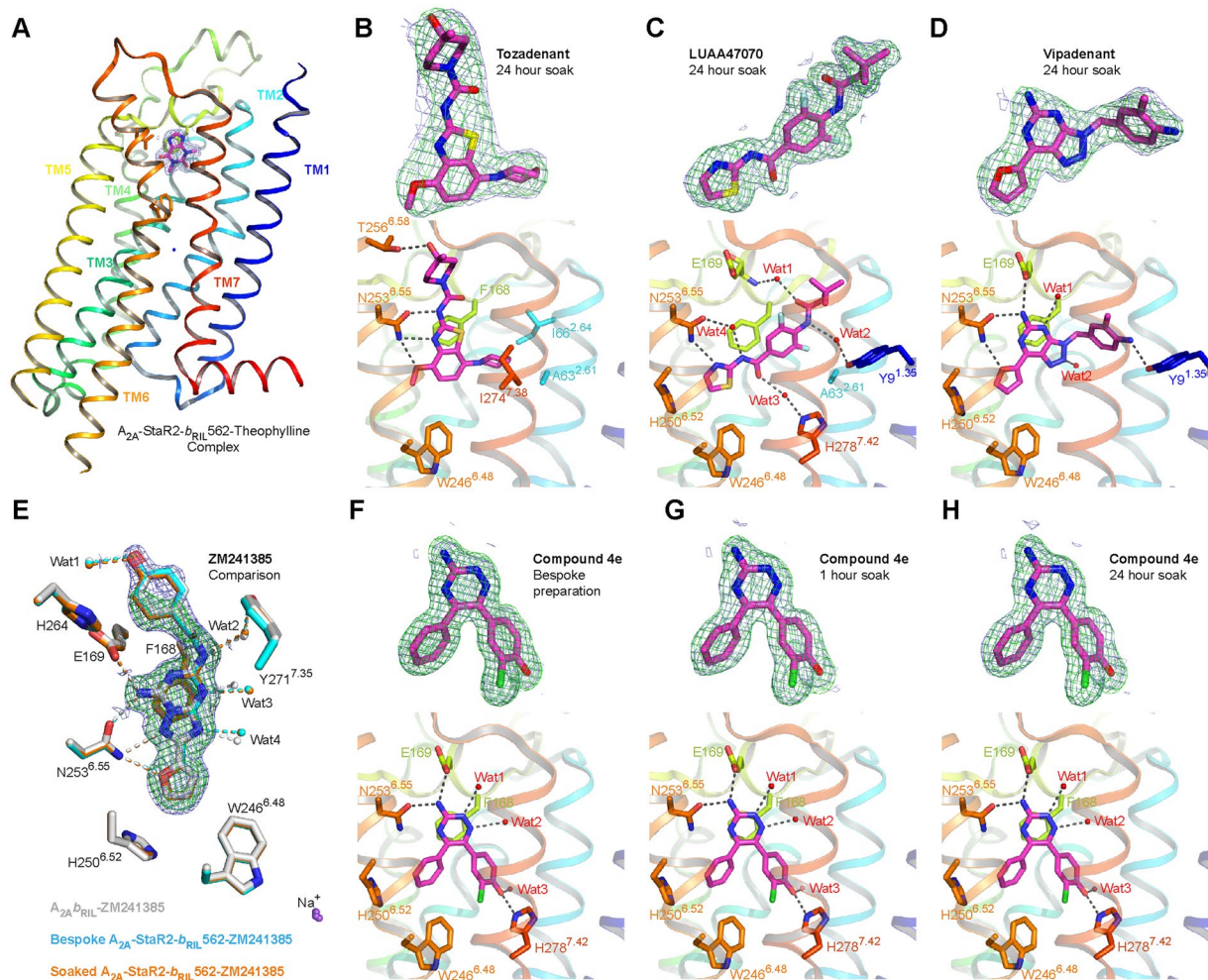


Figure 2. Structure of A_{2A} -StaR2- b_{RIL562} -ligand complexes. **(A)** Structure of the A_{2A} -StaR2- b_{RIL562} -Theophylline complex (PDB: 5MZY) shown in cartoon, with helices coloured differently from blue (helix 1) to red (helix 8). Theophylline is shown as sticks within the 1.0σ contoured $2mFo-dFc$ electron density maps (blue mesh) carved around the ligand. Interesting orthosteric binding site residues are shown as sticks. 1.0σ contoured $2mFo-dFc$ and 3.5σ contoured $mFo-dFc$ ligand omit electron density maps (blue and green meshes respectively) reflecting the quality of ligand (purple sticks) fitting are shown in the top panel, whereas the lower panel provides interaction details between A_{2A} -StaR2- b_{RIL562} binding site residues (sticks) with **Tozadenant** **(B)**, **LUAA47070** **(C)** or **Vipadenant** **(D)**. In these figures, water molecules are represented as red spheres whereas hydrogen bonding is highlighted by dotted lines. An overlay of structures of **ZM241385** in complex with A_{2A} -StaR2- b_{RIL562} from either a bespoke preparation (PDB: 5UI4) (cyan) or from a soaking experiment (orange), and with $A_{2A}b_{RIL562}$ (PDB: 4EIIY) (white) depicts the high degree of conservation in positioning of orthosteric binding site residues **(E)**. Residues and water molecules involved in ligand binding within a 5 \AA radius are represented as sticks and as spheres respectively. Hydrogen bonds are shown as dotted lines and the 1.0σ contoured $2mFo-dFc$ and 3.5σ contoured $mFo-dFc$ ligand omit electron density maps corresponding to **ZM241385** from the soaking experiment are represented as blue and green meshes respectively, carved around the ligand. Similarly electron density maps and interactions are shown for A_{2A} -StaR2- b_{RIL562} -**Compound 4e** generated from bespoke crystallisation **(F)** or from either 1 hour **(G)** or 24 hour **(H)** soaks of A_{2A} -StaR2- b_{RIL562} -Theophylline crystals with **Compound 4e**.

bespoke A_{2A} -StaR2- b_{RIL562} (PDB: 5IU4) or 0.118 \AA (soaked v/s bespoke A_{2A} - b_{RIL562} (PDB: 4EIIY)) (Fig. 2E). Such a high degree of structural conservation across different crystallisation methods (and $A_{2A}R$ constructs) benchmarks and underlines the robustness of the *in meso* soaking system described here.

To determine the feasibility of using the *in meso* soaking method system to support optimisation of novel $A_{2A}R$ antagonists for drug discovery, **Compound 4e**, a 1,2,4-triazine derivative¹⁹, was investigated. **Compound 4e** is a low nanomolar affinity ligand ($pK_D = 9.6$) for $A_{2A}R$ and increases A_{2A} -StaR2- b_{RIL562} stability by $\sim 19^\circ\text{C}$ when compared to *apo* protein (Fig. 1A) and co-crystals were generated using either a bespoke protein preparation or by soaking A_{2A} -StaR2- b_{RIL562} -Theophylline crystals in mother liquor supplemented with **Compound 4e** for 1 or 24 hours (Fig. 1D,E). Crystal morphology remained unchanged regardless of soaking times (Fig. 1D,E) and crystals from these three experiments diffracted to $1.9\text{--}2.1 \text{ \AA}$ in spacegroup $C222_1$. Structures generated from

	Compound 4e (1 hour soak) 5OM1	Compound 4e (24 hour soak) 5OM4	Compound 4e (Bespoke) 5OLZ	Tozadenant (24 hour soak) 5OLO	Vipadenant (24 hour soak) 5OLH	LUAA47070 (24 hour soak) 5OLV	ZM241385 (24 hour soak) 5OLG
Data collection							
Space group	C222 ₁	C222 ₁	C222 ₁	C222 ₁	C222 ₁	C222 ₁	C222 ₁
Cell dimensions							
<i>a</i> , <i>b</i> , <i>c</i> (Å)	39.54, 179.85, 140.32	39.47, 179.11, 140.03	39.37, 179.25, 140.07	39.38, 181.10, 141.77	39.40, 179.33, 141.14	39.43, 180.77, 140.90	39.45, 179.39, 139.60
α , β , γ (°)	90, 90, 90	90, 90, 90	90, 90, 90	90, 90, 90	90, 90, 90	90, 90, 90	90, 90, 90
Resolution (Å)	33.83–2.10 (2.16–2.10) ^a	32.92–2.00 (2.05–2.00) ^a	33.71–1.90 (1.94–1.90) ^a	38.48–3.10 (3.21–3.10) ^a	29.82–2.60 (2.72–2.60) ^a	76.08–2.00 (2.05–2.00) ^a	46.53–1.85 (1.89–1.85) ^a
<i>R</i> _{pin}	0.061 (0.564) ^a	0.059 (0.635) ^a	0.040 (0.583) ^a	0.078 (0.559) ^a	0.097 (0.547) ^a	0.059 (0.624) ^a	0.068 (0.935) ^a
<i>I</i> / σ (<i>I</i>)	10.0 (1.5) ^a	10.3 (1.3) ^a	11.3 (1.4) ^a	8.3 (1.5) ^a	8.3 (1.8) ^a	8.0 (1.3) ^a	7.7 (1.0) ^a
<i>CC</i> _{1/2}	0.997 (0.524) ^a	0.998 (0.439) ^a	0.999 (0.421) ^a	0.997 (0.480) ^a	0.988 (0.519) ^a	0.997 (0.420) ^a	0.994 (0.372) ^a
Completeness (%)	100.0 (100.0) ^a	98.4 (98.8) ^a	99.3 (99.6) ^a	99.9 (100.0) ^a	99.5 (98.7) ^a	98.5 (94.1) ^a	99.7 (100) ^a
Redundancy	6.6 (6.7) ^a	6.3 (6.5) ^a	4.7 (4.8) ^a	5.7 (5.9) ^a	6.9 (5.1) ^a	3.6 (3.7) ^a	6.2 (6.4) ^a
Refinement							
Resolution (Å)	33.83–2.10	32.92–2.00	33.71–1.90	38.48–3.10	29.82–2.60	41.68–2.00	41.31–1.86
No. reflections	56388	63810	74939	9645	15827	34169	41376
<i>R</i> _{work} / <i>R</i> _{free}	0.1882/0.2097	0.1831/0.2049	0.1727/0.1963	0.1987/0.2448	0.2000/0.2487	0.1801/0.2081	0.1921/0.2332
No. atoms							
Protein	3082	3083	3104	2983	3047	3083	3097
Ligand	21	21	21	28	24	24	25
Solvent	687	727	684	397	488	607	597
B factors							
Protein	40.55	39.22	45.33	80.98	43.21	40.19	36.81
Ligand	19.40	17.37	20.13	49.00	21.26	18.28	27.17
Solvent	55.49	56.88	59.69	87.00	51.60	51.83	49.20
R.m.s. deviations							
Bond lengths (Å)	0.002	0.003	0.004	0.002	0.003	0.009	0.014
Bond angles (°)	0.92	0.93	0.99	0.74	0.75	1.19	1.54

Table 1. Data collection and refinement statistics. ^aValues in parentheses are for highest-resolution shell. All data presented above were collected from single crystals except for the A_{2A}-StaR2-*b*_{RIL}562-Vipadenant complex, where data was merged from three different crystals.

bespoke crystallisation or from the soaking experiments were essentially equivalent (r.m.s.d ~0.1 Å over 297 residues). **Compound 4e** was well defined in electron density maps from the resultant three co-structures and binds in the same orientation in the orthosteric site (Fig. 2F–H), displaying similar *B factors* (17.8–19.8 Å²) (Table 1). **Compound 4e** sits lower in the orthosteric site than theophylline, with the triazine ring π stacking against Phe168 from ECL2, while also engaging in polar contacts with an extensive water network. The amine moiety on the triazine ring is further hydrogen-bonded to ECL2 Glu169 and Asn253^{6,55}, whereas the hydroxyl group on the chlorophenol ring makes a hydrogen bond with His278^{7,43}. In the basal region of the orthosteric site, the ligand benzyl ring makes Van der Waals interactions with Trp246^{6,48}.

A pairwise comparison of residues located within 5 Å of all the different liganded structures presented here demonstrates all atom r.m.s.d. values ranging from 0.48 Å (between the A_{2A}-StaR2-*b*_{RIL}562-**Compound 4e** and -LUAA47070 structures) to 1.05 Å (between the A_{2A}-StaR2-*b*_{RIL}562-ZM241385 and -Tozadenant structures). Altogether, most of the mobility stems from Tyr271^{7,35}, involved in water-mediated interactions with ZM241385, and from Glu169 in ECL2 and His264 which adopt different rotamer orientations in the A_{2A}-StaR2-*b*_{RIL}562-Tozadenant structure compared to the other ligand complexes.

In drug development, high-throughput X-ray crystallography expedites the elaboration of novel hits into lead compounds and drug candidates by providing multiple high resolution views of ligand-receptor complexes, which are key for understanding critical intermolecular interactions alongside interpretation of ligand-induced receptor conformational changes²⁷. The accelerated availability of multiple receptor-ligand complexes provides a data-rich starting point for SBDD and medicinal chemistry²⁸ which, when correlated with *in vitro* biological activity, allows rapid incorporation of molecular modifications towards increasing ligand affinity for the binding site or improvement of their absorption, distribution, metabolism, excretion and toxicity (ADMET) properties.

We have demonstrated that an *in meso* ligand soaking methodology can rapidly and efficiently yield multiple high-resolution co-crystal structures from a diverse set of ligands in complex with a given GPCR. Such soaking techniques have also been employed *in-house* for other discovery projects. The method described here has general applicability to further discovery campaigns with stabilised membrane proteins using LCP crystallisation setups, provided high quality crystals exist for the target in complex with low affinity stabilising carrier ligands with fast off-rates.

Methods

StaR generation. The thermostabilisation of the human A_{2A} receptor (resulting in A_{2A}-StaR2) using a mutagenesis approach⁸, has been previously described²⁹.

Expression, membrane preparation and protein purification. The A_{2A} -StaR2- b_{RIL562} construct has been described previously²⁵ and harbours eight thermostabilising mutations (A54L^{2,52}, T88A^{3,36}, R107A^{3,55}, K122A^{4,43}, L202A^{5,63}, L235A^{6,37}, V239A^{6,41} and S277A^{7,42}) as well as a mutation to remove a glycosylation site (N154A). The construct further comprises an Apocytochrome b_{RIL562} fusion between transmembrane helices 5 and 6 and a C-terminal decahistidine tag. The receptor was expressed using the Bac to Bac Expression System (Invitrogen) in *Trichoplusia ni* Tni PRO cells using ESF 921 medium (Expression Systems) supplemented with 5% (v/v) fetal bovine serum (Sigma-Aldrich) and 1% (v/v) Penicillin/Streptomycin (PAA Laboratories). Cells were infected at a density of 2.6×10^6 cells/ml with virus at an approximate multiplicity of infection of 1. Cultures were grown at 27 °C with constant shaking and harvested by centrifugation 48 hours post infection. All subsequent protein purification steps were carried out at 4 °C unless otherwise stated.

For each protein preparation, cells from 2 L cultures were resuspended in 40 mM TRIS buffer at pH 7.6 supplemented with 1 mM EDTA and Complete EDTA-free protease inhibitor cocktail tablets (Roche). Cells were disrupted at ~15 000 psi using a microfluidizer (Processor M-110L Pneumatic, Microfluidics). Membranes pelleted by ultra-centrifugation at 200 000 g for 50 minutes, were subjected to a high salt wash in a buffer containing 40 mM Tris pH 7.6, 1 M NaCl and Complete EDTA-free protease inhibitor cocktail tablets, before they were centrifuged at 200,000 g for 50 minutes. Washed membranes were resuspended in 50 mL 40 mM Tris pH 7.6 supplemented with Complete EDTA-free protease inhibitor cocktail tablets and stored at -80 °C until further use.

Protein preparations intended for soaking experiments were carried out in the presence of theophylline whereas the bespoke preparation of A_{2A} -StaR2- b_{RIL562} in complex with **Compound 4e** was done in the presence of 5 μ M ligand.

Membranes were thawed, resuspended in a total volume of 150 ml with 40 mM Tris-HCl pH 7.6, Complete EDTA-free protease inhibitor cocktail tablets (Roche), 3 mM theophylline (Sigma Aldrich) (or 5 μ M **Compound 4e**), and incubated for 2 hours at room temperature. Membranes were then solubilized by addition of 1.5% n-Decyl- β -D-maltopyranoside (DM, Anatrace), and incubation for 2 hours at 4 °C, followed by centrifugation at 145 000 g for 60 min to harvest solubilised material.

The solubilised material was applied to a 5 ml Ni-NTA (nickel-nitrilotriacetic acid) Superflow cartridge (Qiagen) pre-equilibrated in 40 mM Tris pH 7.4, 200 mM NaCl, 0.15% DM, 1 mM theophylline (or 5 μ M **Compound 4e**). The column was washed with 25 column volumes of buffer 40 mM Tris pH 7.4, 200 mM NaCl, 0.15% DM, 70 mM imidazole, 1 mM theophylline (or 5 μ M **Compound 4e**) and then the protein was eluted with 40 mM Tris pH 7.4, 200 mM NaCl, 0.15% DM, 280 mM imidazole, 1 mM theophylline (or 5 μ M **Compound 4e**).

Collected fractions were analyzed by SDS PAGE and fractions containing A_{2A} -StaR2- b_{RIL562} were pooled and concentrated using an Amicon Ultra Ultracell 50 K ultrafiltration membrane to a final volume of ~800 μ l. The protein sample was ultra-centrifuged at 436 000 g for 10 minutes before being applied to a Superdex200 size exclusion column (GE Healthcare) pre-equilibrated with 40 mM Tris pH 7.4, 200 mM NaCl, 0.15% DM, 1 mM theophylline (or 5 μ M **Compound 4e**). Eluted fractions containing the protein were analyzed by SDS PAGE, pooled and concentrated to ~35 mg/ml using an Amicon Ultra Ultracell 50 K ultrafiltration membrane and subjected to an ultra-centrifugation at 436 000 g prior to crystallisation. Protein concentrations were measured using the DC assay (Bio-Rad), and confirmed using quantitative amino acid analysis.

Thermal unfolding experiments. A_{2A} -StaR2- b_{RIL562} purified in DM in the presence of 500 μ M theophylline was used for thermal unfolding experiments. The protein was diluted in 40 mM Tris pH 7.4, 200 mM NaCl, 0.15% DM to a final concentration of 0.2 mg/ml. Following heavy dilution (~70-fold) of the protein in a buffer without ligand, the sample was considered to be in an *apo*-like state. Samples were supplemented with the respective ligands to a final concentration of 50 μ M, with a final DMSO concentration of 5% (v/v). The control sample was supplemented with DMSO to a final concentration of 5% (v/v). Samples were incubated 30 minutes on ice before being loaded into UV capillaries (NanoTemper Technologies) and experiments were carried out using the Prometheus NT.48. The temperature gradient was set to an +1 °C/min from 20 °C to 90 °C. Protein unfolding was measured by detecting the temperature-dependent change in tryptophan fluorescence at emission wavelengths of 330 and 350 nm. The experiment was repeated four times and data analysed with the one-way analysis of variance (ANOVA) with Dunnett's post-test. T_m values obtained for the three ligands are statistically different from the control sample with $p < 0.001$.

Crystallisation. The A_{2A} -StaR2- b_{RIL562} in complex with either theophylline or **Compound 4e** was crystallized in lipidic cubic phase at 20 °C. Concentrated protein was mixed with monoolein (Nu-Chek) supplemented with 10% (w/w) cholesterol (Sigma Aldrich) and 10 μ M theophylline (or 5 μ M **Compound 4e**) using the twin-syringe method³⁰. The final protein:lipid ratio was 40:60 (w/w). 40 nl boli were dispensed onto 96-well Laminex Glass Bases (Molecular Dimensions Ltd) using a Mosquito LCP crystallization robot (TTP Labtech) and overlaid with 800 nL precipitant solution. Glass bases were sealed using Laminex Film covers (Molecular Dimensions Ltd). 60–80 μ m long plate-shaped crystals grew within 2 weeks in 0.1 M tri-sodium citrate pH 5.3–5.4, 0.05 M sodium thiocyanate, 29–32% PEG400, 2% (v/v) 2,5-hexanediol and 0.5 mM theophylline (or 5 μ M **Compound 4e**).

In meso soaking and crystal harvesting. For soaking experiments, incisions were made into the Laminex cover over base wells containing crystals identified for harvesting and these wells were flooded with 10 μ L mother-liquor supplemented by 1 mM ligand. The crystals are soaked in mother-liquor with a final ligand concentration of 925 μ M, and a final theophylline concentration of 74 μ M. Flooded wells were then re-sealed using Crystal Clear Sealing Tape (Hampton Research), and plates were incubated for 1 hour or 24 hours at 20 °C. Single crystals were mounted in LithoLoops (Molecular Dimensions Ltd) and flash-frozen in liquid nitrogen without the addition of further cryoprotectant.

Diffraction data collection and processing. X-ray diffraction data were measured on a Pilatus 6 M detector at beamline I24 (Diamond Light Source) using a $6 \times 9 \mu\text{m}$ beam size of for crystals of A_{2A} -StaR2- $b_{\text{RIL}}562$ in complex with **Compound 4e**, **Tozadenant** or **LUAA47070**. Complete datasets were acquired from a single crystal for each of these complexes at wavelengths 0.96857 Å (**Compound 4e** and **LUAA47070**) or 0.96862 Å (**Tozadenant**), using an unattenuated beam and 0.2° oscillation per frame, with an exposure of 0.1 second per degree of oscillation. Diffraction data for the A_{2A} -StaR2- $b_{\text{RIL}}562$ -**Vipadenant** complex were acquired from 3 different crystals on an Eiger 16 M detector at beamline X06SA (Swiss Light Source) at a wavelength of 1 Å, using 10% beam transmission and 0.1° oscillation per frame, with an exposure of 1 second per degree of oscillation. The A_{2A} -StaR2- $b_{\text{RIL}}562$ -**ZM241385** data was collected from a single crystal on an Eiger 16 M detector at beamline X06SA at a wavelength of 1 Å, using 20% beam transmission and 0.25° oscillation per frame, with an exposure of 0.24 second per degree of oscillation. Data from individual crystals were integrated using *XDS*³¹, merged and scaled using *AIMLESS*³² from the CCP4 suite³³. Data collection statistics are reported in Table 1.

Structure solution and refinement. The structures of the different A_{2A} -StaR2- $b_{\text{RIL}}562$ -ligand complexes were solved by molecular replacement (MR) with *Phaser*³⁴ using the A_{2A} -StaR2- $b_{\text{RIL}}562$ -theophylline complex structure²⁰ as the search model (PDB code: 5MZJ). Iterative rounds of model refinement performed using *phenix.refine*³⁵, were interspersed with manual model building in *COOT*³⁶. Both xray and B-factor restraint weights were optimised in *phenix.refine*, and 2 TLS groups corresponding to the receptor and to the $b_{\text{RIL}}562$ respectively were defined during refinement. Refinement was with positional and individual isotropic B-factor refinement. The final models were validated using MolProbity³⁷. The final refinement statistics are presented in Table 1. Structure figures were generated using PyMOL³⁸. The three structures of the A_{2A} -StaR2- $b_{\text{RIL}}562$ -**Compound 4e** reported here generated from crystals grown using LCP, are comparable with the previously reported A_{2A} -StaR2-**Compound 4e** structure (PDB: 3UZC)¹⁹ solved from crystals grown using the vapour diffusion technique, with an all atom r.m.s.d. of 0.91 Å over 276 residues.

Data Availability Statement. The data that support the findings of this study are available from the corresponding author upon reasonable request. Co-ordinates and structure factors have been deposited in the Protein Data Bank under the accession codes 5OM1, 5OM4, 5OLZ, 5OLV, 5OLO, 5OLH and 5OLG.

References

- Cooke, R. M., Brown, A. J., Marshall, F. H. & Mason, J. S. Structures of G protein-coupled receptors reveal new opportunities for drug discovery. *Drug discovery today* **20**, 1355–1364, <https://doi.org/10.1016/j.drudis.2015.08.003> (2015).
- Jazayeri, A. *et al.* Extra-helical binding site of a glucagon receptor antagonist. *Nature* **533**, 274–277, <https://doi.org/10.1038/nature17414> (2016).
- Stevens, R. C. *et al.* The GPCR Network: a large-scale collaboration to determine human GPCR structure and function. *Nature reviews. Drug discovery* **12**, 25–34, <https://doi.org/10.1038/nrd3859> (2013).
- Xiang, J. *et al.* Successful Strategies to Determine High-Resolution Structures of GPCRs. *Trends in pharmacological sciences* **37**, 1055–1069, <https://doi.org/10.1016/j.tips.2016.09.009> (2016).
- Congreve, M., Dias, J. M. & Marshall, F. H. Structure-based drug design for G protein-coupled receptors. *Progress in medicinal chemistry* **53**, 1–63, <https://doi.org/10.1016/B978-0-444-63380-4.00001-9> (2014).
- Shoichet, B. K. & Kobilka, B. K. Structure-based drug screening for G-protein-coupled receptors. *Trends in pharmacological sciences* **33**, 268–272, <https://doi.org/10.1016/j.tips.2012.03.007> (2012).
- van Montfort, R. L. & Workman, P. Structure-based design of molecular cancer therapeutics. *Trends in biotechnology* **27**, 315–328, <https://doi.org/10.1016/j.tibtech.2009.02.003> (2009).
- Robertson, N. *et al.* The properties of thermostabilised G protein-coupled receptors (StaRs) and their use in drug discovery. *Neuropharmacology* **60**, 36–44, <https://doi.org/10.1016/j.neuropharm.2010.07.001> (2011).
- Schutz, M. *et al.* Directed evolution of G protein-coupled receptors in yeast for higher functional production in eukaryotic expression hosts. *Scientific reports* **6**, 21508, <https://doi.org/10.1038/srep21508> (2016).
- Scott, D. J., Kummer, L., Egloff, P., Bathgate, R. A. & Pluckthun, A. Improving the apo-state detergent stability of NTS1 with CHES for pharmacological and structural studies. *Biochimica et biophysica acta* **1838**, 2817–2824, <https://doi.org/10.1016/j.bbame.2014.07.015> (2014).
- Miller, J. L. & Tate, C. G. Engineering an ultra-thermostable beta(1)-adrenoceptor. *Journal of molecular biology* **413**, 628–638, <https://doi.org/10.1016/j.jmb.2011.08.057> (2011).
- Alexandrov, A. I., Mileni, M., Chien, E. Y., Hanson, M. A. & Stevens, R. C. Microscale fluorescent thermal stability assay for membrane proteins. *Structure* **16**, 351–359, <https://doi.org/10.1016/j.str.2008.02.004> (2008).
- Yasuda, S. *et al.* Hot-Spot Residues to be Mutated Common in G Protein-Coupled Receptors of Class A: Identification of Thermostabilizing Mutations Followed by Determination of Three-Dimensional Structures for Two Example Receptors. *The journal of physical chemistry. B*, <https://doi.org/10.1021/acs.jpcc.7b02997> (2017).
- Serrano-Vega, M. J., Magnani, F., Shibata, Y. & Tate, C. G. Conformational thermostabilization of the beta1-adrenergic receptor in a detergent-resistant form. *Proceedings of the National Academy of Sciences of the United States of America* **105**, 877–882, <https://doi.org/10.1073/pnas.0711253105> (2008).
- Hollenstein, K. *et al.* Structure of class B GPCR corticotropin-releasing factor receptor 1. *Nature* **499**, 438–443, <https://doi.org/10.1038/nature12357> (2013).
- Dore, A. S. *et al.* Structure of class C GPCR metabotropic glutamate receptor 5 transmembrane domain. *Nature* **511**, 557–562, <https://doi.org/10.1038/nature13396> (2014).
- Christopher, J. A. *et al.* Biophysical fragment screening of the beta1-adrenergic receptor: identification of high affinity arylpiperazine leads using structure-based drug design. *Journal of medicinal chemistry* **56**, 3446–3455, <https://doi.org/10.1021/jm400140q> (2013).
- Segala, E., Errey, J. C., Fiez-Vandal, C., Zhukov, A. & Cooke, R. M. Biosensor-based affinities and binding kinetics of small molecule antagonists to the adenosine A(2A) receptor reconstituted in HDL like particles. *FEBS letters* **589**, 1399–1405, <https://doi.org/10.1016/j.febslet.2015.04.030> (2015).
- Congreve, M. *et al.* Discovery of 1,2,4-triazine derivatives as adenosine A(2A) antagonists using structure based drug design. *Journal of medicinal chemistry* **55**, 1898–1903, <https://doi.org/10.1021/jm201376w> (2012).
- Cheng, R. K. Y. *et al.* Structures of Human A1 and A2A Adenosine Receptors with Xanthines Reveal Determinants of Selectivity. *Structure*, <https://doi.org/10.1016/j.str.2017.06.012> (2017).
- Flohr, A., Moreau, J.-L., Poli, S. M., Riemer, C. & Steward, L. 4-hydroxy-4-methyl-piperidine-1-carboxylic acid (4-methoxy-7-morpholin-4-yl-benzothiazol-2-yl)-amide. US 20050261289 A1 (2008).

22. Sams, A. G. *et al.* Discovery of phosphoric acid mono-{2-[(E/Z)-4-(3,3-dimethyl-butylamino)-3,5-difluoro-benzoylimino]-thiazol-3-ylmethyl} ester (Lu AA47070): a phosphonooxymethylene prodrug of a potent and selective hA(2A) receptor antagonist. *Journal of medicinal chemistry* **54**, 751–764, <https://doi.org/10.1021/jm1008659> (2011).
23. Gillespie, R. J. *et al.* Antagonists of the human A(2A) adenosine receptor. 4. *Design, synthesis, and preclinical evaluation of 7-aryltriazolo[4,5-d]pyrimidines*. *Journal of medicinal chemistry* **52**, 33–47, <https://doi.org/10.1021/jm800961g> (2009).
24. Poucher, S. M. *et al.* The *in vitro* pharmacology of ZM 241385, a potent, non-xanthine A2a selective adenosine receptor antagonist. *British journal of pharmacology* **115**, 1096–1102 (1995).
25. Segala, E. *et al.* Controlling the Dissociation of Ligands from the Adenosine A2A Receptor through Modulation of Salt Bridge Strength. *Journal of medicinal chemistry* **59**, 6470–6479, <https://doi.org/10.1021/acs.jmedchem.6b00653> (2016).
26. Liu, W. *et al.* Structural basis for allosteric regulation of GPCRs by sodium ions. *Science* **337**, 232–236, <https://doi.org/10.1126/science.1219218> (2012).
27. Blundell, T. L., Jhoti, H. & Abell, C. High-throughput crystallography for lead discovery in drug design. *Nature reviews. Drug discovery* **1**, 45–54, <https://doi.org/10.1038/nrd706> (2002).
28. Ferreira, L. G., Dos Santos, R. N., Oliva, G. & Andricopulo, A. D. Molecular docking and structure-based drug design strategies. *Molecules* **20**, 13384–13421, <https://doi.org/10.3390/molecules200713384> (2015).
29. Dore, A. S. *et al.* Structure of the adenosine A(2A) receptor in complex with ZM241385 and the xanthines XAC and caffeine. *Structure* **19**, 1283–1293, <https://doi.org/10.1016/j.str.2011.06.014> (2011).
30. Caffrey, M. & Cherezov, V. Crystallizing membrane proteins using lipidic mesophases. *Nature protocols* **4**, 706–731, <https://doi.org/10.1038/nprot.2009.31> (2009).
31. Kabsch, W. Xds. *Acta crystallographica. Section D, Biological crystallography* **66**, 125–132, <https://doi.org/10.1107/S0907444909047337> (2010).
32. Evans, P. Scaling and assessment of data quality. *Acta crystallographica. Section D, Biological crystallography* **62**, 72–82, <https://doi.org/10.1107/S0907444905036693> (2006).
33. Winn, M. D. *et al.* Overview of the CCP4 suite and current developments. *Acta crystallographica. Section D, Biological crystallography* **67**, 235–242, <https://doi.org/10.1107/S0907444910045749> (2011).
34. McCoy, A. J. *et al.* Phaser crystallographic software. *Journal of applied crystallography* **40**, 658–674, <https://doi.org/10.1107/S0021889807021206> (2007).
35. Afonine, P. V. *et al.* Towards automated crystallographic structure refinement with phenix.refine. *Acta crystallographica. Section D, Biological crystallography* **68**, 352–367, <https://doi.org/10.1107/S0907444912001308> (2012).
36. Emsley, P., Lohkamp, B., Scott, W. G. & Cowtan, K. Features and development of Coot. *Acta crystallographica. Section D, Biological crystallography* **66**, 486–501, <https://doi.org/10.1107/S0907444910007493> (2010).
37. Chen, V. B. *et al.* MolProbity: all-atom structure validation for macromolecular crystallography. *Acta crystallographica. Section D, Biological crystallography* **66**, 12–21, <https://doi.org/10.1107/S0907444909042073> (2010).
38. Schrodinger, L. L. C. *The PyMOL Molecular Graphics System, Version 1.8* (2015).

Acknowledgements

The research leading to these results has received support from the Innovative Medicines Initiative Joint Undertaking under K4DD (www.k4dd.eu), grant agreement no. 115366, resources of which are composed of financial contribution from the European Union's Seventh Framework Programme (FP7/2007–2013) and EFPIA companies' in kind contribution. More info: www.imi.europa.eu. We thank D. Axford, R. Owen and D. Sherrell at I24, Diamond Light Source, Oxford, UK and M. Wang at beamline X06SA, Swiss Light Source, Villigen, Switzerland for technical support. We thank colleagues at Heptares Therapeutics Ltd. for suggestions and comments.

Author Contributions

R.K.Y.C. devised initial soaking experiments, performed LCP crystallization, designed crystal optimization, performed *in meso* soaking experiments, collected and processed X-ray diffraction data, solved and refined the structures. E.S. established the protein expression and purification protocols and performed LCP crystallization. T.G. performed and optimized protein purification. P.R. and T.G. optimized and performed *in meso* soaking experiments, collected and processed X-ray diffraction data and solved and refined structures. P.R. refined the final structures. Project management was carried out by A.S.D., J.C.E., G.A.B., R.M.C., and F.H.M. The manuscript was prepared by P.R., A.S.D. and F.H.M.

Additional Information

Competing Interests: The authors are shareholders of Sosei Group Corporation and declare competing financial interests.

Publisher's note: Springer Nature remains neutral with regard to jurisdictional claims in published maps and institutional affiliations.



Open Access This article is licensed under a Creative Commons Attribution 4.0 International License, which permits use, sharing, adaptation, distribution and reproduction in any medium or format, as long as you give appropriate credit to the original author(s) and the source, provide a link to the Creative Commons license, and indicate if changes were made. The images or other third party material in this article are included in the article's Creative Commons license, unless indicated otherwise in a credit line to the material. If material is not included in the article's Creative Commons license and your intended use is not permitted by statutory regulation or exceeds the permitted use, you will need to obtain permission directly from the copyright holder. To view a copy of this license, visit <http://creativecommons.org/licenses/by/4.0/>.

© The Author(s) 2017